

Performance Analysis of a Novel Architecture of Cs₂AgBiBr₆-based Tandem perovskite photovoltaics

SHREYUS GOUTHAM KUMAR¹, SHYLESH K B², UDAY C², PRASHANTH C R³

¹Department of Electronics and Communication Engineering, PES University-EC Campus, Karnataka, India, and Research Scholar in Department of ETE, Dr. AIT, Karnataka, INDIA.

²Department of Electronics and Communication Engineering, PES University-EC Campus, Karnataka, INDIA

^bDept. of Electronics and Communication, SJB Institute of Technology, Affiliated to VTU, Bengaluru, Karnataka 560060, INDIA

¹Corresponding Author: shreyasgouatham@pes.edu

Abstract: Organic-inorganic hybrid perovskites can be used in solar cells with a single junction to achieve more than 25.5% efficiency. Optimizing the absorber layer (perovskite film) or investigating cutting-edge device designs, such as tandem-based solar cells that combine perovskite and silicon, can improve the device's power conversion efficiency (PCE). The overall power conversion efficiency (PCE) of a combination of silicon and perovskite solar cells can be increased above the Shockley-Queisser limit, which is the theoretical efficiency limit for single-junction solar cells. Utilizing a wider spectrum of solar light allows for this. This work shows how to model and optimize a stand-alone Cs₂AgBiBr₆ perovskite solar cell. Then, using SCAPS-1D, it merges that model with a crystalline silicon (c-Si) solar cell to simulate a tandem assembly. The goal of the project was to place a perovskite solar cell on top of a high-efficiency c-Si solar cell with a four-terminal (4T) structure to increase its efficiency. The simulation yielded an output voltage of 1.5V and a short-circuit current density of 23.07 MA/cm² for the Cs₂AgBiBr₆ perovskite solar cell, which translated into a power conversion efficiency of **29.66%**. The tandem arrangement exhibited a significantly higher power conversion efficiency (**43.76%**) than individual cells. The findings indicate that the Cs₂AgBiBr₆ perovskite solar cell can be used in tandem systems with c-Si solar cells to obtain very high levels of efficiency. This work offers significant new insights into the design of effective perovskite e-Si tandem solar cells

Keywords: Filtered Spectrum, Perovskite, SCAPS-1D, Tandem, Solar cell

Received: May 26, 2024. Revised: January 15, 2025. Accepted: March 19, 2025. Published: June 4, 2025.

1. Introduction:

In an attempt to improve solar cell efficiency, multi-junction cells—also referred to as tandem cells—that are made up of solar cells with different band gaps are being investigated. Researchers want to exceed the Shockley-Queisser model's 31% power conversion efficiency (PCE) limit for single-junction devices. As the world's energy demand is expected to rise from 15 TW in 2011 to an estimated 30 TW by 2050, this strategy is considered essential [1]–[3].

Tandem systems benefit from top absorber materials with a wide bandgap (WBG) and bottom absorbers with a narrow bandgap (NBG). With silicon (Si) serving as the bottom absorber and III-V compound semiconductor-based materials serving as the top absorber, current generation

multi-junction tandem solar cells (MJ-TSCs) have reached a notable 39% conversion efficiency under 1 sun conditions [4]. However, the high cost and precise production requirements associated with III-V compounds pose barriers to their widespread commercial adoption [5].

The advent of perovskite materials has had an impact on the research landscape focusing on III-V materials over the past ten years. Benefits of perovskites include higher absorption coefficient, affordability, ease of production, longer carrier diffusion length, reduced carrier effective mass, and bandgap tunability. Perovskite materials are therefore thought to be possible replacements.

In an effort to lower the levelized cost of electricity (LCOE) and increase conversion efficiency in solar cell technology, two-junction tandem solar cells (2-

T TSCs) are being studied by researchers. With a PCE of 13.7%, Mailoa et al. (2015) made history by creating the first two-terminal (2-T) perovskite/Si TSC. Zheng et al. made further improvements by using SnO_2 as the interconnecting layer (ICL) and electron transport layer (ETL) of the top cell. This led to a PCE increase of 17.10% on a 16 cm^2 tandem solar cell (TSC) [8].

Though halide double perovskites, or elpasolites, have been known to science for almost a century, the photovoltaic community has recently been more interested in them [9]. The double perovskite structure of these compounds is typified by the alternating octahedra BX_6 and $\text{B}'\text{X}_6$, which share a corner. This structure's arrangement of two distinct cations, B and B', creates a three-dimensional superstructure known as rock-salt ordering [10]. The overall charge of the combined B and B' cations must be +4 in order to preserve charge neutrality. This criterion opens up new options within the halide double perovskite family by making it easier to explore combinations combining $1+/3+$ cations.

Two main factors are driving research on $\text{A}_2\text{BB}'\text{X}_6$ perovskites in the photovoltaics industry. In the first, the goal is to maintain the advantageous 3D network that is made up of inorganic corner-sharing octahedra. Concurrently, there is a desire to investigate Pb replacement with less hazardous materials. The goal of this method is to preserve the special qualities of 3D APbX_3 materials, such as their strong light absorption, low band gap ($\approx 1.6 \text{ eV}$), extended lifetime of photogenerated electrons and holes, and evenly distributed carrier effective masses. Further increasing the adaptability of these materials is the ability to expand the spectrum of atoms that can be added to the B sites by utilizing double perovskites [11]

2. Device Structure

In the assessment of tandem solar cell performance, a common practice involves the separate simulation of the top and bottom sub-cells. In this modelling approach, the tunnel junction is assumed to be free of imperfections, and both optical and electrical losses at the interfaces are disregarded, as outlined in the standard multi-junction modelling model

[12]–[15]. Tandem solar cell systems often feature perovskite solar cells as the top cell and silicon solar cells as the bottom cell.

The $\text{Cs}_2\text{AgBiBr}_6$ perovskite solar cell used in this experiment has a band gap of 1.64 eV and a thickness of $1.08 \mu\text{m}$, which together produce a high absorption coefficient and open-circuit voltage (V_{oc}). A hole-transport layer (HTL) and an electron-transport layer (ETL) surround the perovskite layer. The HTL is made of NiO with a band gap of 3.7 and a thickness of $2 \mu\text{m}$. It has remarkable hole-transport and stability characteristics. With a band gap of 3.6 and a thickness of $0.030 \mu\text{m}$, the SnO_2 used to make the ETL has a low bandgap and strong electron mobility.

Crystalline silicon (c-Si) cells, which have a high open-circuit voltage, low resistance, and long-term stability, make up the bottom cell. The bandgap and voltage of the c-Si cell are carefully adjusted to match those of the perovskite cell in order to maximize energy capture. Utilizing the high absorption coefficient of the perovskite cell, the high open-circuit voltage and low resistance of the c-Si cell, the advantageous features of the ETL (low bandgap and high electron mobility), and the effective hole-transport characteristics of the HTL, this tandem configuration turns out to be a very effective photovoltaic device. The structure of non-lead PSC is depicted in Fig 1.

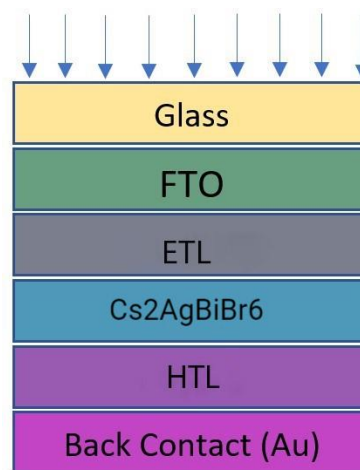


Fig 1: Design of the non-lead PSC

Table I: Reference Perovskite Solar Cell Input Parameters

Parameters	FTO	TiO ₂	Cs ₂ AgBiBr ₆	NiO
Thickness (um)	0.05	0.1	0.6	0.1
E _g (eV)	3.6	3.26	1.72	3.8
χ (eV)	4.0	4.2	4.19	1.46
ε _r	9.0	10.0	5.8	10.7
N _c (cm ⁻³)	2.2x10 ¹⁸	2x10 ¹⁷	1x10 ¹⁶	2.8x10 ¹⁹
N _v (cm ⁻³)	1.8x10 ¹⁹	6x10 ¹⁷	1x10 ¹⁶	1x10 ¹⁹
μ _n (cm ² /Vs)	100	100	11.81	12
μ _p (cm ² /Vs)	25	25	0.49	2.8
N _d (cm ⁻³)	1x10 ¹⁸	1x10 ¹⁷	-	-
N _a (cm ⁻³)	-	-	1x10 ¹⁸	1x10 ¹⁹

Table I contains a list of the input values for the top cell, which were taken from the reference [31]. Now to get the best ETL and HTL materials such that the cell functioning is maximized, various ETL materials such as (AZO, SnO₂, CdS, IGZO, PCBM)

whose parameters are got from various published reports [17], [20]–[23] which are summarized in Table II are substituted and the simulation is carried out following the same method

Table II Properties of different ETL materials

Parameters	CdS	IGZO	SnO ₂	PCBM	AZO
E _g (eV)	2.4	3.05	3.30	2	3.3
χ (eV)	4.2	4.16	4	3.9	3.8
ε _r	10	10	9	3.9	9
N _c (cm ⁻³)	2.2x10 ¹⁸	5x10 ¹⁸	2.2x10 ¹⁷	2.5 x10 ²¹	4 x10 ¹⁸
N _v (cm ⁻³)	1.8x10 ¹⁹	5x10 ¹⁸	2.2x10 ¹⁶	2.5 x10 ²¹	1x10 ¹⁹
μ _n (cm ² /Vs)	100	15	200	0.2	100
μ _p (cm ² /Vs)	25	0.1	80	0.2	25
N _d (cm ⁻³)	1x10 ¹⁷	1x10 ¹⁸	1x10 ¹⁷	2.93 x10 ¹⁷	1x10 ¹⁸
N _a (cm ⁻³)	0	0	0	0	0
N _t (cm ⁻³)	1x10 ¹⁷	1x10 ¹⁵	1x10 ¹⁵	1x10 ¹⁵	1x10 ¹⁵

Various HTL materials such as (Cu₂O, CuI, PEDOT: PSS, CuSbS₂, NiO, and CuSCN) whose parameters are also got from various published

reports [16]–[20] which are summarized in Table III are substituted and the simulation is done in the same method.

Table III: Properties of different HTL materials

Parameters	Cu ₂ O	CuI	CuSCN	NiO	CuSbS ₂
E _g (eV)	2.17	2.98	3.4	3.8	1.58
χ (eV)	3.2	2.1	1.9	1.46	4.2
ε _r	6.6	6.5	10	11.7	14.6
N _c (cm ⁻³)	2.5x10 ²⁰	2.8x10 ¹⁹	1.7x10 ¹⁹	2.5x10 ²⁰	2x10 ¹⁸
N _v (cm ⁻³)	2.5x10 ²⁰	1x10 ¹⁹	2.5x10 ²¹	2.5x10 ²⁰	1x10 ¹⁹
μ _n (cm ² /Vs)	80	0.00017	0.00015	2.8	49
μ _p (cm ² /Vs)	80	0.0002	0.1	2.8	49
N _d (cm ⁻³)	0	0	0	0	0
N _a (cm ⁻³)	1x10 ¹⁸	1x10 ¹⁸	1x10 ¹⁸	1x10 ¹⁸	1.38x10 ¹⁸
N _t (cm ⁻³)	1x10 ¹⁵	1x10 ¹⁵	1x10 ¹⁴	1x10 ¹⁵	1x10 ¹⁴

3. Methodology

3.1 Numerical Methods

In recent times, simulation treatments for the optimization and evaluation of various parameters have attracted the majority of interest in solar research. Planar heterojunction OIP solar cells have been numerically simulated in the current study using SCAPS 1D. JV curve, power conversion efficiency, projected energy band gap, etc. are performance metrics that may be evaluated by using the continuity equation for solving Poisson's equation. The PCE, FF, J_{sc}, and V_{oc} are also calculated using these curves.

$$\frac{d}{dz} \left[-\epsilon(z) \frac{d\phi}{dz} \right] = q [p(z) - n(z) + N_D^+(z) - N_A^-(z) + p_t(z) - n_t(z)]$$

$$\frac{dp_n}{dt} = G_p - \frac{p_n - p_{n0}}{\tau_p} + p_n \mu_p \frac{d\xi}{dz} + \mu_p \xi \frac{dp_n}{dz} + D_p \frac{d^2 p_n}{dz^2}$$

$$\frac{dn_p}{dt} = G_n - \frac{n_p - n_{p0}}{\tau_n} + n_p \mu_n \frac{d\xi}{dz} + \mu_n \xi \frac{dn_p}{dz} + D_n \frac{d^2 n_p}{dz^2}$$

Furthermore, it is important to note that the solar cell solely absorbs photons with energy greater than the semiconductors' band gaps, resulting in the production of holes and electron pairs [25]. The shortest wavelength of photons with sufficient

energy to produce carriers is determined by E_g. Hence, the cut-off wavelength is given by:

$$\lambda = \frac{1240}{E_g(\text{eV})} (\text{nm}) \quad - (1)$$

At J= 0 mAcm⁻², The greatest voltage that a solar cell can generate, known as the open-circuit voltage (V_{oc}), can be represented as follows:

$$V_{oc} = \frac{kT}{q} \ln \left(\frac{J_{sc}}{J_0} + 1 \right) \quad - (2)$$

where J₀ is the saturation point current density, temperature is given by T, q is the carrier charge, and k is the Boltzmann constant. The FF is given by:

$$FF = \frac{P_m}{V_{oc} \cdot J_{sc}} \quad (3)$$

Once more, Green [28] provides a precise calculation for determining the FF:

$$FF = \frac{v_{oc} - \ln(v_{oc} + 0.72)}{v_{oc} + 1} \quad - (4)$$

where $v_{oc} = \left(\frac{V_{oc}}{V_{th}} \right)$ is normalized V_{oc}

The theoretical FF was to be determined in ideal conditions in the current work, though. The largest FF values come from Equation 5, which ignores resistive losses [28]. Moreover, the maximum power point of a solar cell's power output to power input ratio is indicated as follows:

$$\eta = \frac{P_m}{P_m \cdot A} \quad - (5)$$

where P_{in} denotes the radiation's intensity at the incidence and A denotes the area. Once more, when the voltage across a solar cell is zero, the short-circuit current is equivalent to the electricity that is flowing through the cell. It is supplied by and depends on the solar spectrum being used.

$$J_{sc} = q \int_{E_g}^{\infty} \frac{dN_{ph}}{dh\nu} d(h\nu) \quad - (6)$$

The Varshni relationship [29]–[31] yields the T-based bandgap at random temperature, T.

$$E_g(T) = E_g(0) - \frac{\alpha T^2}{(T + \beta)^2} \quad - (7)$$

where α and β are constants, the crucial parameter that determines the J_{sc} is electron mobility, while electron affinity depends on the material. By altering the material's qualities, it can be altered.

Furthermore, the simulation results will be extracted using Eqs. 1-8.

4. Results and Discussion

A tandem device is characterized by a sequential arrangement of two-cell combinations, forming a tandem structure with two terminals. Consequently, the open-circuit voltage (V_{oc}) of the tandem cell is the cumulative sum of its sub-cell voltages. It is noteworthy that the short-circuit current (J_{sc}) of the entire device is constrained by the lowest junction current among the sub-cells, thereby setting a limit on the overall short-circuit current of the tandem device [32]. The subsequent section will encompass simulations for both the complete tandem device and the individual cells.

The reference PSC is optimized in the next section by choosing suitable ETL and HTL materials, maximizing the thickness of the absorber layer, examining the impact of defect densities in the absorber layer, maximizing the thickness of particular ETL and HTL materials, and lastly examining the impact of the PSC's bandgap. Summary of a previously published article using $Cs_2AgBiBr_6$ as an absorber layer is shown in Table IV

Table IV: Device parameter comparison of $Cs_2AgBiBr_6$ - based PSC with earlier reported outcomes

Device Architecture	JSC (mA/cm ²)	VOC (V)	FF (%)	PCE (%)
ITO/CuNiO/ $Cs_2AgBiBr_6$ /C60/BCP/Ag[24]	3.19	1.01	69	2.23
FTO/TiO ₂ / $Cs_2AgBiBr_6$ /Spiro-OMeTAD/MoO ₃ /Ag [25]	3.28	1.01	65	2.51
FTO/TiO ₂ / $Cs_2AgBiBr_6$ /N719/Spiro-OMeTAD/Ag [26]	5.13	1.06	51	2.84
ITO/SnO ₂ / $Cs_2AgBiBr_6$ /Spiro-OMeTAD/Au [27]	11.4	0.92	60.93	6.37
FTO/TiO ₂ / $Cs_2AgBiBr_6$ /Cu ₂ O/Au.[28]	11.45	1.50	42.14	7.25
ITO/SnO ₂ / $Cs_2AgBiBr_6$ / P3HT/Au [29]	6.39	2.02	90	11.32
FTO/ZnO/ $Cs_2AgBiBr_6$ /NiO/Au.[30]	20.69	1.29	81.72	21.88
Ni/NiOx/ $Cs_2AgBiBr_6$ /TiO ₂ /FTO/Al [31] [reference]	21.46	1.33	88.53	25.38
FTO/SnO₂/$Cs_2AgBiBr_6$/ NiO/Au [This Work]	23.07	1.5	88.43	29.66

4.1 Selection of HTL layer

The material layer of a solar cell called the hole transport layer (HTL) facilitates the transfer of positive charges, or holes, from the absorber layer to the electrical interface. The HTL can raise the overall efficiency of the solar cell by reducing the possibility of hole and electron recombination at the interface between the light-absorbing layer and the electrical contact. If holes and electrons recombine at this contact, the solar cell's efficiency will drop since the latter cannot contribute to the current generated by the former. The HTL provides a path for the holes to follow in order to reach the electrical contact, which helps to prevent this recombination and increase the efficiency of the solar cell. Table 2 shows the simulation results of different HTLs. The bar plot represents the various HTLs' efficiency as shown in Fig 2.

Table 2: Simulation results of various HTLs

	Cu ₂ O	CuI	CuSCN	CuSbS ₂	NiO
Voc	1.3208	0.971	1.25	1.157	1.504
Jsc	23.07	23.07	23.074	23.76	23.074
FF	78.96	74.87	78.10	83.71	85.43
PCE	24.06	16.78	22.54	23.03	29.66

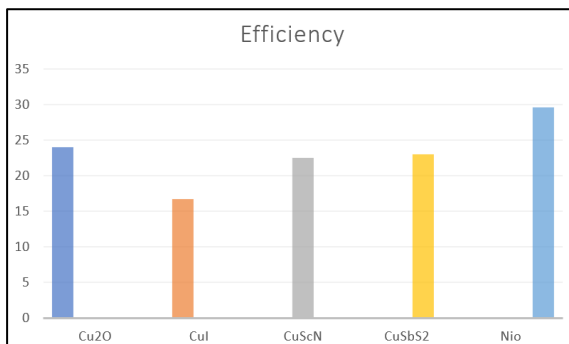


Fig 2: Efficiency of various HTL materials

4.2 Selection of ETL layer

The job of the electron transport layer is to transfer electrons created in the absorber layer when sunlight splits into electron-hole pairs and moves them to the front contact of the photovoltaic solar cell. Moreover, it prevents the holes from passing

through the layer of absorber and coming in contact with the head contact. As a result, we looked at the efficiency, open-circuit voltage, and current density of several ETLs. Table 3 shows the simulation results of different ETLs. The bar plot presents the various HTLs' efficiency as shown in Fig 3.

Table 3: Simulation results of various ETLs

	PCBM	AZO	CdS	IGZO	SnO ₂
Voc	1.5208	0.9512	1.34	1.157	1.504
Jsc	23.06	24.07	22.12	23.76	23.07
FF	78.96	77.87	74.10	83.71	85.43
PCE	23.06	19.78	20.43	23.03	29.66

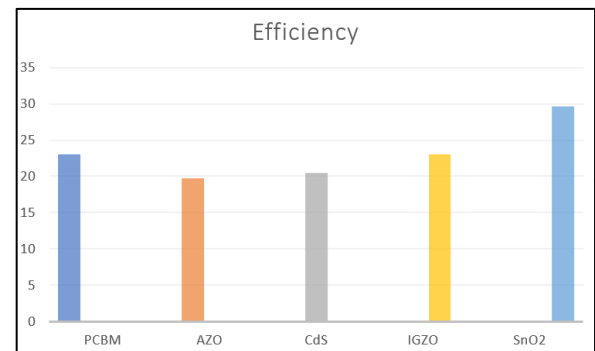


Fig 3: Efficiency of various ETL materials

The effect of various ETL materials on the quantum efficiency (QE) of the PSCs are shown in Fig. 3. AZO has the lowest PCE, and should not be utilized to construct lead-free PSCs, according to our simulation. SnO₂ has the highest Jsc and PCE when compared to all the other ETLs in the table. Therefore considering SnO₂ as ETL helps in achieving higher efficiency.

4.3 Effect of Absorber Layer Thickness

The thickness of the AL is an important factor in determining PSC performance [33]. Because it absorbs incoming photons and produces charge carriers, the absorber layer (AL) in perovskite solar cells (PSCs) is important to solar cell performance. The durability and diffusion length of photo-generated carriers are directly impacted by the quality of the AL, which is determined by parameters including film shape [34, 35]. To absorb the most photons possible, the AL thickness must be carefully selected. If the thickness is too thick, the reverse saturation current may be reduced.

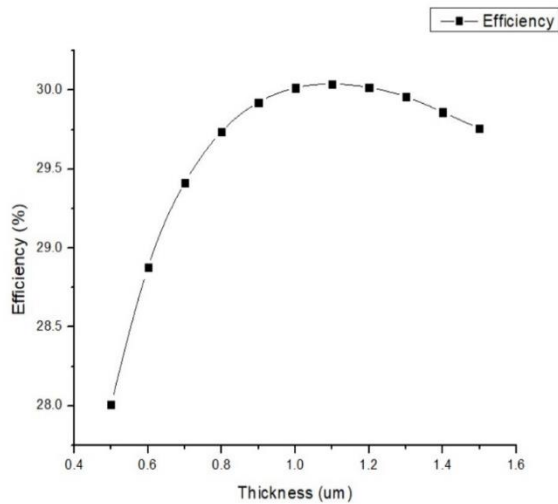


Fig 4: Impact of thickness variation

Fig 4 illustrates the impact of varying absorber thickness, ranging from 500 to 1100 nm, on PSC performance, while keeping all other input properties constant. Observations reveal a systematic decrease in V_{oc} (from 1.5061 to 1.5 V) with increasing AL thickness, while the average AL thickness concurrently enhances J_{sc} (from 22.66 to 23.07). The efficiency exhibits a peak value of 29.66 at 1100 nm, accompanied by a decrease in fill factor (FF) from 89.28 to 85.43%. However, as the AL thickness increases, the recombination of charge carriers within the material intensifies, leading to a decline in efficiency [36]. Hence, an optimal thickness of 400 nm for $Cs_2AgBiBr_6$ is identified for achieving high efficiency [36].

4.4 Effect of Absorber Layer Bandgap

Fig 5 shows the effect of absorber layer bandgap on PSC's efficiency. By altering the energy gap of the deflecting parts, optical deflection can be regulated to create a highly efficient device [37]. The energy gap of AL in PSC devices, however, plays a significant role in the eye twitching. $Cs_2AgBiBr_6$'s thickness was set at 1100 nm, while all other parameters stayed the same. Because of the absorber level's 1.64 eV bandgap (E_g), this design can provide a maximum PCE of 29.66% and a maximum FF of 85.43%.

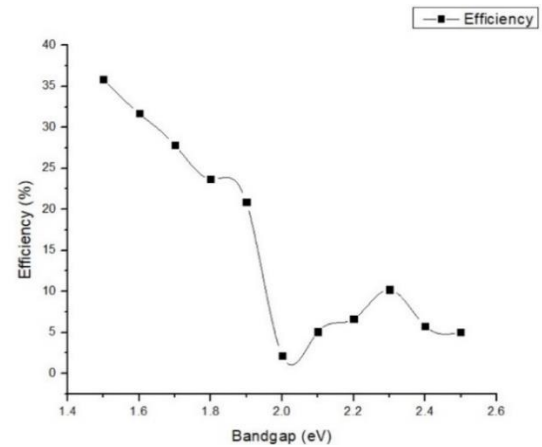


Fig 5: Effect of Absorber Layer Bandgap

4.5 Effect of Absorber Layer Defect Density

Defects in any perovskite material are inevitable and might take the form of point defects such as gaps, vacancies, Schottky and Frenkel defects, etc. On numbers and surfaces, other flaws like reflections and grain boundaries can also be seen. The process of self-doping perovskite layers, which captures charge carriers and encourages nonradiative recombination, can also result in impurity defects [38]. Furthermore, high defect density impairs PSC performance. From 10^{13} to 10^{17} cm^{-3} , the AL fault density has been tuned and altered in order to fully comprehend its effect. Fig 6 illustrates the impact of absorber layer defect density. V_{oc} essentially stays unchanged. When the defect density rises from 10^{16} to 10^{17} , J_{sc} experiences a fall in absorber layer concentration from 22.11 to 12.30 mA/cm^2 . According to the graph, PCE drops from 29.66 to 3.07% and FF drops from 85.43 to 22.94%.

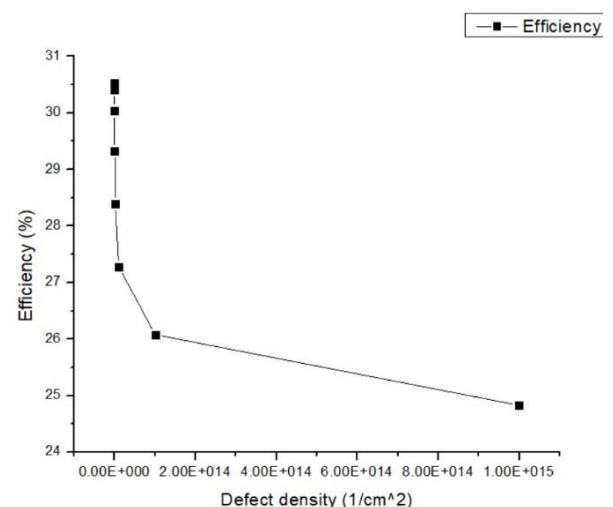


Fig 6: Effect of Absorber Layer Defect Density

4.6. The Absorber Layer's Electron Affinity's Impact

Fig 7 illustrates the impact of absorber layer's electron affinity. The amount of energy needed to change a neutral atom into a negative ion is known as a molecule's electron affinity. One key factor impacting performance is the electrical affinity of the perovskite material, which can have a significant impact on device performance [37]. We conduct 3.6 to 4.2 eV and various electron withdrawals of $\text{Cs}_2\text{AgBiBr}_6$ up to the device configuration in order to ascertain the impact of electron withdrawal on the PSC performance parameters. A rise in V_{oc} may transpire gradually as a result of elevated electron absorption. Additionally, PCE increased linearly from 24.68 to 29.66%.

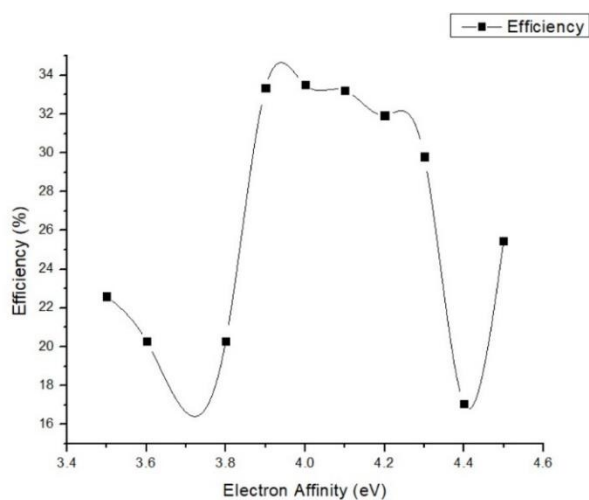


Fig 7: The Absorber Layer's Electron Affinity's Impact

4.7 Effect of ETL Thickness

The tool's performance is significantly influenced by the thickness of the ETL. Fig 8 shows the effect of ETL thickness. In addition to serving as channels for electron transmission from the AL, the ETL separates the electrode from the absorber layer [38]. ETL size can make it more difficult for charged ions (holes and electrons) to access the anode and cathode electrodes by increasing series resistance, which might result in recombination [39]. However, if ETL size is too reduced (below 50 nm) at electrode between a and absorber, To explore the effect of modifying the ETL size on the trap performane, which is too thin to provide efficient separation, we simulated the trap when varying the

ETL size from 30 to 150 nm. The highest level of efficiency attained was 29.66%.

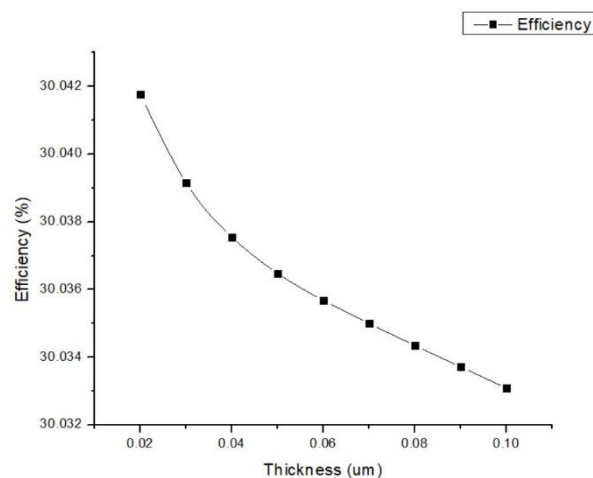


Fig 8: Effect of ETL Thickness

4.8. Impact of HTL/Absorber Interface Defect Density

Interfacial faults, or charge recombination centers, are caused by structural mismatches between the two components or by the introduction of external stimuli in PSCs [40]. The impact of the method is also significant for third-generation solar cells (especially from the mouthpiece). Furthermore, non-radiative losses resulting from positive potential at heterojunctions between perovskite/charge extraction layers (HTL or ETL) and perovskite absorber defects cause V_{oc} loss. The interaction between many PSC layers also affects device performance and long-term stability. When grid-assisted non-radiative reconnection is employed with an interface that has many defects/voids or grid conditions, voltage and current losses result. In order to comprehend the impact of defect density at the HTL/absorber layer interface, we adjust this number from 10^{10} to 10^{21} cm^{-3} . The HTL/AL interface's fault density has minimal bearing on the PSC's performance. As the faults increase from 10^{10} to 10^{18} cm^{-3} , a progressive decline in the performance coefficients is seen. Significant variations in the interfacial defect density (from 10^{18} to 10^{21} cm^{-3}) had no effect on these values. Fig 9 shows the impact of HTL/Absorber interface defect density

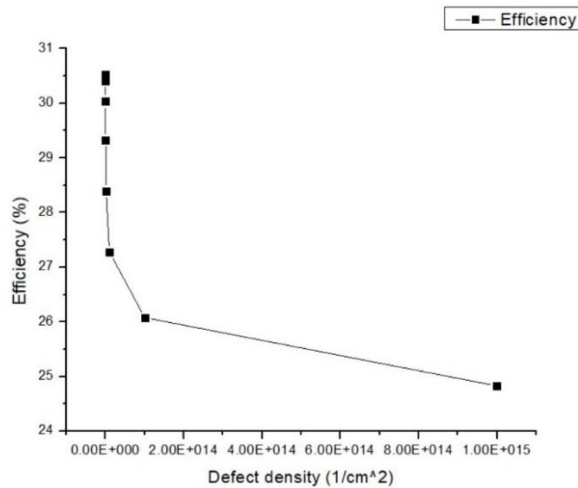


Fig 9: Impact of HTL/Absorber Interface Defect Density

4.9. Impact of ETL/Absorber Interface Defect Density

Forward network failures have a greater impact on a PSC device's performance than surface network issues. This behavior can be explained by the perovskite material's larger absorption coefficient, which increases photon absorption close to the front contact and, as a result, creates more pairs of electron holes there. At this point, it is understood how charge carriers differ from network-assisted recombination. Consequently, we discover that issues with the frontal interface significantly affect the functionality of the gadget. Consequently, we must concentrate on debugging the front end. A number of mechanics, including ionic liquids [41], anti-relationship [42], graphene-based, juicy-based, and probe-based probes -based on the [43] - have been created for the passive process of inter-form defects. By contrast, there is a significant decrease in J_{sc} (24.20 to 22.99 mA/cm²), which is caused by the defect of increasing bio density (from 10^{16} to 10^{18} cm⁻³). The J_{sc} variation of the first four steps (10^{10} to 10^{18} cm⁻³) associated with interface defect density variation is relatively insignificant. Furthermore, as the SnO₂/Cs₂AgBiBr₆ interface defect density increases, a progressive decline in FF and PCE is also seen; FF fell from 85.43 to 73.15% and PCE fell from 29.66 to 24.63% as shown in fig 10. Fig 10 illustrates the impact of ETL/Absorber interface defect density

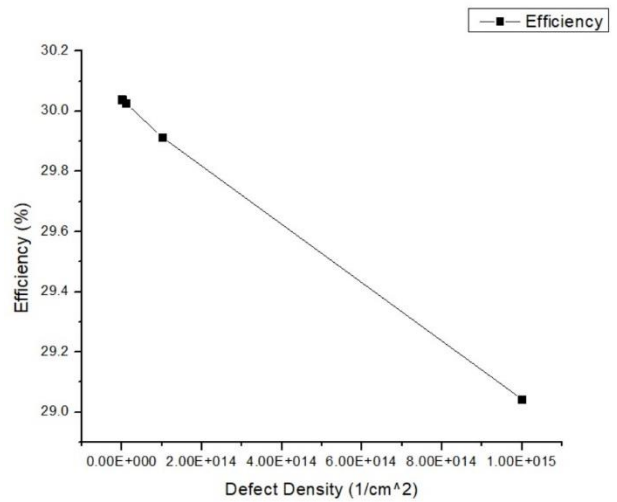


Fig 10: Impact of ETL/Absorber Interface Defect Density

4.10 Effect of Operating temperature on device performance

The current investigation's general operating temperature throughout simulation was 300 K. PSCs can, however, have their temperature altered during production, characterisation, and external usage. Season, height, latitude, and the time of day in a particular place all have an impact on the operating temperature. The performance of a PSC device is influenced by its operating temperature as shown in fig 11. The primary source of the PCE's reduction with rising temperature is a drop in the Voc. Voc is being observed to drop with increasing or decrease in temperature.

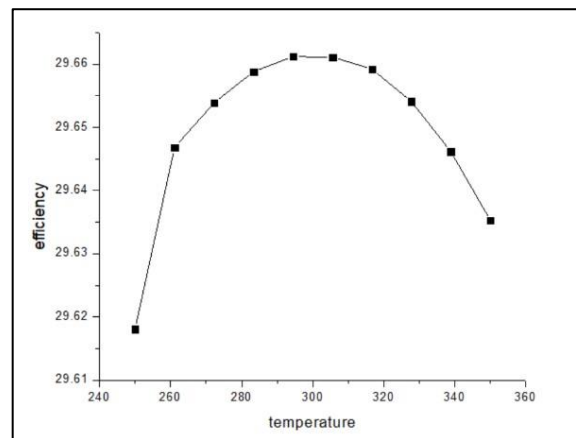


Fig 11: The way that operating temperature affects the functionality of a device

4.11 Simulation of Tandem Solar cell:

The lower-energy photons in the mechanically stacked tandem perovskite solar cell are captured by the c-Si bottom cell, while the higher-energy

photons are captured by the perovskite top cell. The perovskite layer is a potential material for photovoltaics because of its high light absorption coefficient, quick charge carrier mobility, and inexpensive cost. In contrast, the c-Si bottom cell is a proven material that has been commercialized for a considerable amount of time in the solar sector.

The tandem perovskite solar cell can overcome some of the drawbacks of single-junction cells and reach high conversion efficiencies by combining these two elements in a mechanically stacked structure. The commercialization of mechanically stacked tandem perovskite solar cells is contingent upon the development of robust and scalable production procedures, as the stability and long-term performance of perovskite materials remain to be explored.

A simple method has been used to simulate the tandem cell using the SCAPS-1-D simulation software. We conducted our investigation using mechanically stacked two-terminal tandem cells, which are effectively two diodes connected in series. We also applied the current matching condition between the top and bottom cells [44]. Even in the scenario where the voltage is obtained by adding the voltages of individual cells, the cell with the lower Jsc dominates the current-limiting criterion of the overall tandem arrangement. To match the current, either Jsc variation or maximum power current density (JMP) variation is employed.

References

- [1] Sharma, Surbhi, Soumen Basu, Nagaraj P. Shetti, and Tejraj M. Aminabhavi. "Waste-to-energy nexus for circular economy and environmental protection: Recent trends in hydrogen energy." *Science of the Total Environment* 713 (2020): 136633. [\[CrossRef\]](#) [\[Google Scholar\]](#)
- [2] Glatt, Moritz F., Li Yi, Gülsüm Mert, Barbara S. Linke, and Jan C. Aurich. "Technical product-service systems: analysis and reduction of the cumulative energy demand." *Journal of cleaner*

Table 4: Results of Simulations

Cell	Voc	Jsc	FF (%)	PCE (%)
(Top Cell)	1.5	23.07	88.43	29.66
c-Si (Bottom Cell)	0.74	21.28	85.25	22.78
(Tandem)	1.48	14.94	89.05	43.76

We adjust the bottom cell's thickness to determine the current matching point. According to Table 4, we get an efficiency of **43.76%** in our simulation.

5. Conclusion:

This research studies non-lead PSCs with Cs₂AgBiBr₆ perovskite as the absorber layer using SCAPS modelling. First, the best materials for the ETL and HTL, which are SnO₂ and NiO, respectively, are determined. Subsequently, the effects of absorber layer thickness, absorber layer defect density, absorber layer band-gap, SnO₂ thickness, and NiO thickness on PSC performance are investigated. The PSC configuration is glass substrate/FTO/SnO₂/Cs₂AgBiBr₆/NiO/Au.

According to the models, the absorber layer should have an optimal defect density of 1×10^{13} cm⁻³. Any higher defect densities will cause a decrease in solar cell performance since more recombination sites will form. Using this PSC as the top cell and c-Si as the bottom cell, we have also simulated the tandem structure. The efficiency has increased from 29.66% in a single structure to **43.76%** in tandem, as we have shown. The results of this study will contribute to the development of effective and non-lead PSCs, increasing the utilization of solar, wave, and wind energy as sustainable energy sources.

production 206 (2019): 727-740. [\[CrossRef\]](#) [\[Google Scholar\]](#)

[3] Seker, Sukran, and Nezir Aydin. "Hydrogen production facility location selection for Black Sea using entropy based TOPSIS under IVPF environment." *International Journal of Hydrogen Energy* 45, no. 32 (2020): 15855-15868. [\[CrossRef\]](#) [\[Google Scholar\]](#)

[4] Green, Martin, Ewan Dunlop, Jochen Hohl-Ebinger, Masahiro Yoshita, Nikos Kopidakis, and

- Xiaoqing Hao. "Solar cell efficiency tables (version 57)." *Progress in photovoltaics: research and applications* 29, no. 1 (2021): 3-15. [\[CrossRef\]](#) [\[Google Scholar\]](#)
- [5] Leijtens, Tomas, Kevin A. Bush, Rohit Prasanna, and Michael D. McGehee. "Opportunities and challenges for tandem solar cells using metal halide perovskite semiconductors." *Nature Energy* 3, no. 10 (2018): 828-838. [\[CrossRef\]](#) [\[Google Scholar\]](#)
- [6] Yu, Zhengshan J., Joe V. Carpenter III, and Zachary C. Holman. "Techno-economic viability of silicon-based tandem photovoltaic modules in the United States." *Nature Energy* 3, no. 9 (2018): 747-753. [\[CrossRef\]](#) [\[Google Scholar\]](#)
- [7] Mailoa, Jonathan P., Colin D. Bailie, Eric C. Johlin, Eric T. Hoke, Austin J. Akey, William H. Nguyen, Michael D. McGehee, and Tonio Buonassisi. "A 2-terminal perovskite/silicon multijunction solar cell enabled by a silicon tunnel junction." *Applied Physics Letters* 106, no. 12 (2015). Mailoa, Jonathan P., Colin D. Bailie, Eric C. Johlin, Eric T. Hoke, Austin J. Akey, William H. Nguyen, Michael D. McGehee, and Tonio Buonassisi. "A 2-terminal perovskite/silicon multijunction solar cell enabled by a silicon tunnel junction." *Applied Physics Letters* 106, no. 12 (2015). [\[CrossRef\]](#) [\[Google Scholar\]](#)
- [8] Zheng, Jianghui, Cho Fai Jonathan Lau, Hamid Mehrvarz, Fa-Jun Ma, Yajie Jiang, Xiaofan Deng, Anastasia Soeriyadi et al. "Large area efficient interface layer free monolithic perovskite/homo-junction-silicon tandem solar cell with over 20% efficiency." *Energy & Environmental Science* 11, no. 9 (2018): 2432-2443. [\[CrossRef\]](#) [\[Google Scholar\]](#)
- [9] Meyer, Gerd. "The synthesis and structures of complex rare-earth halides." *Progress in Solid State Chemistry* 14, no. 3 (1982): 141-219. [\[CrossRef\]](#) [\[Google Scholar\]](#)
- [10] Slavney, Adam H., Rebecca W. Smaha, Ian C. Smith, Adam Jaffe, Daiki Umeyama, and Hemamala I. Karunadasa. "Chemical approaches to addressing the instability and toxicity of lead-halide perovskite absorbers." *Inorganic chemistry* 56, no. 1 (2017): 46-55. [\[CrossRef\]](#) [\[Google Scholar\]](#)
- [11] Jodlowski, AlexanderD, Daily Rodríguez-Padrón, Rafael Luque, and Gustavo de Miguel. "Alternative perovskites for photovoltaics." *Advanced Energy Materials* 8, no. 21 (2018): 1703120. [\[CrossRef\]](#) [\[Google Scholar\]](#)
- [12] Kim, Kihwan, Jihye Gwak, Seung Kyu Ahn, Young-Joo Eo, Joo Hyung Park, Jun-Sik Cho, Min Gu Kang, Hee-Eun Song, and Jae Ho Yun. "Simulations of chalcopyrite/c-Si tandem cells using SCAPS-1D." *Solar energy* 145 (2017): 52-58. [\[CrossRef\]](#) [\[Google Scholar\]](#)
- [13] Kim, Kihwan, Jin Su Yoo, Seung Kyu Ahn, Young-Joo Eo, Jun-Sik Cho, Jihye Gwak, and Jae Ho Yun. "Performance prediction of chalcopyrite-based dual-junction tandem solar cells." *Solar Energy* 155 (2017): 167-177. [\[CrossRef\]](#) [\[Google Scholar\]](#)
- [14] Gupta, Goutam Kumar, and Ambesh Dixit. "Theoretical studies of single and tandem Cu₂ZnSn (S/Se) 4 junction solar cells for enhanced efficiency." *Optical Materials* 82 (2018): 11-20. [\[CrossRef\]](#) [\[Google Scholar\]](#)
- [15] Madan, Jaya, Rahul Pandey, and Rajnish Sharma. "Device simulation of 17.3% efficient lead-free all-perovskite tandem solar cell." *Solar energy* 197 (2020): 212-221. [\[CrossRef\]](#) [\[Google Scholar\]](#)
- [16] Baig, Faisal, Yousaf Hameed Khattak, Bernabe Mari, Saira Beg, Abrar Ahmed, and Khurram Khan. "Efficiency enhancement of CH₃NH₃SnI₃ solar cells by device modeling." *Journal of Electronic Materials* 47 (2018): 5275-5282.
- [17] Azri, Faiza, Afak Meftah, Nouredine Sengouga, and Amjad Meftah. "Electron and hole transport layers optimization by numerical simulation of a perovskite solar cell." *Solar energy* 181 (2019): 372-378. [\[CrossRef\]](#) [\[Google Scholar\]](#)
- [18] Minemoto, Takashi, and Masashi Murata. "Impact of work function of back contact of perovskite solar cells without hole transport material analyzed by device simulation." *Current Applied Physics* 14, no. 11 (2014): 1428-1433. [\[CrossRef\]](#) [\[Google Scholar\]](#)
- [19] Teimouri, R., and R. Mohammadpour. "Potential application of CuSbS₂ as the hole

transport material in perovskite solar cell: a simulation study." *Superlattices and Microstructures* 118 (2018): 116-122. [\[CrossRef\]](#) [\[Google Scholar\]](#)

[20] Lin, Lingyan, Linqin Jiang, Ping Li, Baodian Fan, and Yu Qiu. "A modeled perovskite solar cell structure with a Cu₂O hole-transporting layer enabling over 20% efficiency by low-cost low-temperature processing." *Journal of Physics and Chemistry of Solids* 124 (2019): 205-211. [\[CrossRef\]](#) [\[Google Scholar\]](#)

[21] Lakhdar, Nacereddine, and Abdelkader Hima. "Electron transport material effect on performance of perovskite solar cells based on CH₃NH₃GeI₃." *Optical Materials* 99 (2020): 109517. [\[CrossRef\]](#) [\[Google Scholar\]](#)

[22] Lin, Ling-yan, Lin-qin Jiang, Yu Qiu, and Baodian Fan. "Analysis of Sb₂Se₃/CdS based photovoltaic cell: A numerical simulation approach." *Journal of physics and chemistry of solids* 122 (2018): 19-24. [\[CrossRef\]](#) [\[Google Scholar\]](#)

[23] Lin, Hsi-Kuei, Jia-Xing Li, Hao-Cheng Wang, Yu-Wei Su, Kaung-Hsiung Wu, and Kung-Hwa Wei. "Dual nanocomposite carrier transport layers enhance the efficiency of planar perovskite photovoltaics." *RSC advances* 8, no. 23 (2018): 12526-12534. [\[CrossRef\]](#) [\[Google Scholar\]](#)

[24] Gao, Weiyin, Chenxin Ran, Jun Xi, Bo Jiao, Wenwen Zhang, Mincai Wu, Xun Hou, and Zhaoxin Wu. "High-quality Cs₂AgBiBr₆ double perovskite film for lead-free inverted planar heterojunction solar cells with 2.2% efficiency." *ChemPhysChem* 19, no. 14 (2018): 1696-1700. [\[CrossRef\]](#) [\[Google Scholar\]](#)

[25] Igbari, Femi, Rui Wang, Zhao-Kui Wang, Xing-Juan Ma, Qiang Wang, Kai-Li Wang, Yue Zhang, Liang-Sheng Liao, and Yang Yang. "Composition stoichiometry of Cs₂AgBiBr₆ films for highly efficient lead-free perovskite solar cells." *Nano letters* 19, no. 3 (2019): 2066-2073. [\[CrossRef\]](#) [\[Google Scholar\]](#)

[26] Yang, Xiaoqing, Yonghui Chen, Pengyun Liu, Huimin Xiang, Wei Wang, Ran Ran, Wei Zhou, and Zongping Shao. "Simultaneous power conversion efficiency and stability enhancement of Cs₂AgBiBr₆ lead-free inorganic perovskite solar

cell through adopting a multifunctional dye interlayer." *Advanced Functional Materials* 30, no. 23 (2020): 2001557. [\[CrossRef\]](#) [\[Google Scholar\]](#)

[27] Zhang, Zeyu, Qingde Sun, Yue Lu, Feng Lu, Xulin Mu, Su-Huai Wei, and Manling Sui. "Hydrogenated Cs₂AgBiBr₆ for significantly improved efficiency of lead-free inorganic double perovskite solar cell." *Nature communications* 13, no. 1 (2022): 3397. [\[CrossRef\]](#) [\[Google Scholar\]](#)

[28] Islam, Md Tohidul, Md Rafsun Jani, Syed Muhammad Al Amin, Md Shifat Us Sami, Kazi Md Shorowordi, Mohammad Istiaque Hossain, Mohan Devgun, Shaestagir Chowdhury, Sankha Banerje, and Saquib Ahmed. "Numerical simulation studies of a fully inorganic Cs₂AgBiBr₆ perovskite solar device." *Optical Materials* 105 (2020): 109957. [\[CrossRef\]](#) [\[Google Scholar\]](#)

[29] Mohandes, Aminreza, Mahmood Moradi, and Hamid Nadgaran. "Numerical simulation of inorganic Cs₂AgBiBr₆ as a lead-free perovskite using device simulation SCAPS-1D." *Optical and Quantum Electronics* 53 (2021): 1-22. [\[CrossRef\]](#) [\[Google Scholar\]](#)

[30] Alkhamash, Hend I., M. Mottakin, Md Mosaddek Hossen, Md Akhtaruzzaman, and Mohammad Junaebur Rashid. "Design and defect study of Cs₂AgBiBr₆ double perovskite solar cell using suitable charge transport layers." *Semiconductor Science and Technology* 38, no. 1 (2022): 015005. [\[CrossRef\]](#) [\[Google Scholar\]](#)

[31] Iftexhar, Md Raghif, Md Golam Rabbani, Adnan Hosen, Md Saiful Islam, Md Suruz Mian, and Sheikh Rashel Al Ahmed. "Simulating the electrical characteristics of a highly efficient Cs₂AgBiBr₆-based perovskite solar cell with NiO x hole transport layer." In *2022 International Conference on Advancement in Electrical and Electronic Engineering (ICAEEE)*, pp. 1-4. IEEE, 2022. [\[CrossRef\]](#) [\[Google Scholar\]](#)

[32] Larsen-Olsen, Thue T., Thomas R. Andersen, Birgitta Andreasen, Arvid PL Böttiger, Eva Bundgaard, Kion Norrman, Jens W. Andreasen, Mikkel Jørgensen, and Frederik C. Krebs. "Roll-to-roll processed polymer tandem solar cells partially processed from water." *Solar Energy Materials and Solar Cells* 97 (2012): 43-49. [\[CrossRef\]](#) [\[Google Scholar\]](#)

- [33] Du, Hui-Jing, Wei-Chao Wang, and Jian-Zhuo Zhu. "Device simulation of lead-free $\text{CH}_3\text{NH}_3\text{SnI}_3$ perovskite solar cells with high efficiency." *Chinese Physics B* 25, no. 10 (2016): 108802. [\[CrossRef\]](#) [\[Google Scholar\]](#)
- [34] Kim, Hobeom, Kyung-Geun Lim, and Tae-Woo Lee. "Planar heterojunction organometal halide perovskite solar cells: roles of interfacial layers." *Energy & Environmental Science* 9, no. 1 (2016): 12-30. [\[CrossRef\]](#) [\[Google Scholar\]](#)
- [35] Barbé, Jérémy, Max L. Tietze, Marios Neophytou, Banavoth Murali, Erkki Alarousu, Abdulrahman El Labban, Mutalifu Abulikemu et al. "Amorphous tin oxide as a low-temperature-processed electron-transport layer for organic and hybrid perovskite solar cells." *ACS applied materials & interfaces* 9, no. 13 (2017): 11828-11836. [\[CrossRef\]](#) [\[Google Scholar\]](#)
- [36] Salah, Mostafa M., Mohamed Abouelatta, Ahmed Shaker, Kamel M. Hassan, and Ahmed Saeed. "A comprehensive simulation study of hybrid halide perovskite solar cell with copper oxide as HTM." *Semiconductor Science and Technology* 34, no. 11 (2019): 115009. [\[CrossRef\]](#) [\[Google Scholar\]](#)
- [37] Jayan, K. Deepthi, and Varkey Sebastian. "Comparative performance analysis of mixed halide perovskite solar cells with different transport layers and back metal contacts." *Semiconductor Science and Technology* 36, no. 6 (2021): 065010. [\[CrossRef\]](#) [\[Google Scholar\]](#)
- [38] Raoui, Yassine, Hamid Ez-Zahraouy, Najim Tahiri, Omar El Bounagui, Shahzada Ahmad, and Samrana Kazim. "Performance analysis of MAPbI_3 based perovskite solar cells employing diverse charge selective contacts: Simulation study." *Solar Energy* 193 (2019): 948-955. [\[CrossRef\]](#) [\[Google Scholar\]](#)
- [39] HOSSEINI, Seyyedreza, Nagihan Delibaş, Mahsa Bahramgour, Alireza Tabatabaei Mashayekh, and Aligholi NIAIE. "Performance comparison of different hole transport layer configurations in a perovskite-based solar cell using SCAPS-1D simulation." *Avrupa Bilim ve Teknoloji Dergisi* 31 (2021): 121-126. [\[CrossRef\]](#) [\[Google Scholar\]](#)
- [40] Basyoni, Marwa Sayed Salem, Mostafa M. Salah, Mohamed Mousa, Ahmed Shaker, Abdelhalim Zekry, Mohamed Abouelatta, Mohammad T. Alshammari, Kawther A. Al-Dhlan, and Christian Gontrand. "On the investigation of interface defects of solar cells: lead-based vs lead-free perovskite." *IEEE Access* 9 (2021): 130221-130232. [\[CrossRef\]](#) [\[Google Scholar\]](#)
- [41] Shahiduzzaman, Md, Ersan Y. Muslih, AK Mahmud Hasan, LiangLe Wang, Shoko Fukaya, Masahiro Nakano, Makoto Karakawa et al. "The benefits of ionic liquids for the fabrication of efficient and stable perovskite photovoltaics." *Chemical Engineering Journal* 411 (2021): 128461. [\[CrossRef\]](#) [\[Google Scholar\]](#)
- [42] Taylor, Alexander D., Qing Sun, Katelyn P. Goetz, Qingzhi An, Tim Schramm, Yvonne Hofstetter, Maximillian Litterst, Fabian Paulus, and Yana Vaynzof. "A general approach to high-efficiency perovskite solar cells by any antisolvent." *Nature communications* 12, no. 1 (2021): 1878. [\[CrossRef\]](#) [\[Google Scholar\]](#)
- [43] Shao, Shuyan, and Maria Antonietta Loi. "The role of the interfaces in perovskite solar cells." *Advanced Materials Interfaces* 7, no. 1 (2020): 1901469. [\[CrossRef\]](#) [\[Google Scholar\]](#)
- [44] Ulbrich, C., C. Zahren, A. Gerber, B. Blank, T. Merdzhanova, A. Gordijn, and U. Rau. "Matching of silicon thin-film tandem solar cells for maximum power output." *International journal of photoenergy* 2013 (2013). [\[CrossRef\]](#) [\[Google Scholar\]](#)